Vortex flow structures and interactions for the optimum thrust efficiency of a heaving airfoil at different mean angles of attack

Martín-Alcántara, A.,[1] Fernandez-Feria, R.[1] and Sanmiguel-Rojas, E.[2]

[1]Universidad de Málaga, Andalucía Tech, E. T. S. Ingeniería Industrial, Dr Ortiz Ramos s/n, 29071 Málaga, Spain

[2]Area de Ingeniería Mecánica, E. Politécnica Superior, Universidad de Córdoba, Campus de Rabanales, 14071 Córdoba, Spain

Abstract

The thrust efficiency of a two-dimensional heaving airfoil is studied computationally for a low Reynolds number using a vortex force decomposition. The auxiliary potentials that separate the total vortex force into lift and drag (or thrust) are obtained analytically by using an elliptic airfoil. With these auxiliary potentials, the added-mass components of the lift and drag (or thrust) coefficients are also obtained analytically for any heaving motion of the airfoil and for any value of the mean angle of attack α. The contributions of the leading- and trailing-edge vortices to the thrust during their down- and up-stroke evolutions are computed quantitatively with this formulation for different dimensionless frequencies and heave amplitudes (St_c and St_a), and for several values of α. Very different types of flows, periodic, quasi-periodic and chaotic, are described as St_c, St_a and α are varied. The optimum values of these parameters for maximum thrust efficiency are obtained, and explained in terms of the interactions between the vortices and the forces exerted by them on the airfoil. As in previous numerical and experimental studies on flapping flight at low Reynolds numbers, the optimum thrust efficiency is reached for intermediate frequencies (St_c slightly smaller than one) and a heave amplitude corresponding to an advance ratio close to unity. The optimal mean angle of attack found is zero. The corresponding flow is periodic, but it becomes chaotic and with smaller average thrust efficiency as $|\alpha|$ becomes slightly different from zero.

I. INTRODUCTION

The unsteady aerodynamics of oscillating airfoils at the low Reynolds number range of interest for small flying animals (mostly insects) has been widely studied theoretically, numerically and experimentally.[1] The main motivation of many of these studies has been the understanding of the flow mechanisms by which the lift is greatly enhanced in relation to the predictions of the quasi-steady aerodynamic theory, and the mechanisms by which thrust or propulsion is generated. Traditionally, these studies were aimed to the understanding of the biomechanics of insect (and small birds and mammals) flight.[2–5] But the interest in the unsteady aerodynamics of flapping flight has significantly grown in recent years in relation to the design of Micro Aerial Vehicles (MAVs), that take advantage of the accumulated knowledge on animal flight.[6–10]

Here we focus on the thrust generation by an oscillating airfoil at low Reynolds numbers. Particularly on the characterization of the vortical flow structures responsible for the maximum thrust efficiency at selected non-dimensional frequencies and amplitudes of the oscillations. We consider the two-dimensional (2D) and incompressible viscous flow around a plunging airfoil at different mean angles of attack. This simplified problem, with only heaving motion, has been widely considered as an appropriate simple model to understand the flow mechanisms which are responsible for thrust generation in flapping flight and swimming. It has been known for a long time that net thrust is characterized by a reversed von Kármán vortex street behind the heaving airfoil,[11,12] with vortices rotating in the opposite direction of the well known drag-producing von Kármán vortex street. Different kinds of spatial patterns of vortices have been identified in several forms of propulsion by aquatic animals.[13–16] In addition, in many of the proposed thrust mechanisms, the leading-edge vortex (LEV) generated during the wing-beat plays an important role. It is well known that the high lift coefficients characterizing most insects flight is due to the low-pressure regions inside the LEV generated temporarily after a sudden change in the effective local angle of attack during flapping.[16–25] To optimize this effect most insects fly at the limit of dynamic stall to generate a prominent LEV. The relevance of the LEV for high efficiency thrust and propulsion by a pure heaving motion was first acknowledged and studied in relation to simple models for fish swimming.[26–28] It was already known that the efficiency of thrust generation by a flapping airfoil is mainly governed by a Strouhal number based on the amplitude and

frequency of the oscillations (St_a defined in the next section).[29–31] For very low St_a, below a threshold of about 0.03, only drag is produced by the oscillating airfoil.[31] For large frequencies for a given amplitude, when $St_a \sim 0.06$, net thrust is generated by the inversion of the vortices in the von Kármán vortex wake behind the heaving airfoil.[30–32] Experimental and numerical results show that, in a wide range of Reynolds numbers (Re, also defined in the next section), the optimal efficiency for thrust generation is reached in an intermediate range of St_a, between 0.12 and 0.20, approximately, which is thus selected by many swimming and flying animals.[29,33–35] By the way, these experimental results contrast the potential theory results for small-amplitude oscillations, predicting that propulsion efficiency is maximized as the frequency goes to zero,[36,37] whence the relevance of viscous effects in modelling the thrust generated by a heaving airfoil at the relevant Reynolds numbers of interest. This flapping frequency selected for optimum thrust efficiency has been identified with the frequency of maximum spatial amplification of the wake, based on linear stability analyses of the wake mean velocity profile,[29,38] and with the natural shedding frequency of the airfoil.[34] Also, this frequency range observed in biological propulsion has been correlated to the range of limiting dimensionless time for optimal vortex formation by the flapping appendage.[39]

It has been shown that the thrust efficiency of a flapping airfoil depends on the interactions between LEV and trailing-edge vortex (TEV),[26,27] the efficiency being larger when they interact constructively leading to two vortices deposited per stroke. This situation occurs in the range of St_a mentioned above. Wang[40] demonstrated, using 2D numerical simulations for a heaving elliptic airfoil and relating the resulting forces to those generated by the LEV in a single stroke, that this preferred range of St_a is connected with maximizing the effective local angle of attack allowed for the low range of Reynolds number considered. But, in addition to St_a, which is a combination of the frequency and amplitude of the oscillations, there exists another degree of freedom, characterized by the reduced frequency (k) or the related Strouhal number based on the flapping frequency only (St_c defined in the next section along with k), which has to be taken into account. Wang[40] related the range of St_c for optimum thrust efficiency to the equilibrium between the time scales for LEV growth and shedding. The obtained value around 0.7 is consistent with data for many birds and insects flight in a wide range of Reynolds numbers.[3,41] In a more detailed numerical study on the vortex structure of the 2D flow around a heaving airfoil at low Reynolds number, Lewin and Haj-Hariri[38] showed that the timing of the separation of the LEV is crucial to the

heaving efficiency, with the optimum thrust occurring when the LEV remains attached for the duration of each stroke. These authors concluded, in agreement with a previous work,[27] that high propulsion efficiencies correspond to the positive reinforcement of the TEV by the LEV. They also found aperiodic and asymmetric (deflected wake) solutions in some ranges of the parameters St_a and St_c (related to kh and k, respectively, in their notation, see next section). The wake patterns depended on whether or not the LEV is shed, and on how the LEV interacts with the TEV (reinforcing or attenuating it). The numerical simulations by Lewin and Haj-Hariri[38] produced aperiodic results when both St_a and St_c were sufficiently high. The mechanisms of the wake deflection in a 2D heaving airfoil, caused by the LEV-TEV interaction, and their connection to the aperiodic flows generated at high St_a even in a symmetrical and periodic heaving motion, have been more recently studied by several authors.[42–45] For instance, the detailed experimental results by Lua et al.[43] for a heaving elliptic airfoil shed further light on the relation between the different LEV-TEV interactions, as St_a and St_c are varied, with the different structures of the wake. But neither of these experimental and numerical studies analyzed quantitatively the effect that the successively generated LEVs and TEVs, and their interactions, have on the thrust of the heaving airfoil. We think that this quantitative analysis is very relevant to understand the vortex configuration for optimum thrust efficiency.

Thus, to explain better all the above phenomena affecting the thrust efficiency of a heaving airfoil, we study in this work the connection between the LEV and the TEV dynamics with the thrust efficiency quantitatively by using a vortex force decomposition, originally developed by Chang,[46] in a 2D numerical simulation of the flow. This formulation provides the quantitative contribution of each vortex flow structure, such as the LEV and the TEV, to the lift and drag or thrust at any instant of time (see also Refs.[47,48]). In order to be able to obtain analytically the auxiliary potentials that separate the vortex force into lift and drag (or thrust), we use an elliptic airfoil, as in many previous numerical works. In addition, in the present work we also consider the effect of mean angles of attack α different from zero in the thrust efficiency of the heaving airfoil, which has not been taken into account in previous works. The vertical asymmetry introduced by $\alpha \neq 0$ changes dramatically the structure of the flow and thrust efficiency, even for small $|\alpha|$. In short, we consider quantitatively the effect of the LEV-TEV interaction, the LEV splitting, stretching, convection and diffusion, and other vortex dynamics mechanisms in the thrust efficiency of a heaving airfoil

for different values of St_a, St_c and α for a given (relatively small) value of the Reynolds number of interest in insects and MAVs flight.

The remainder of the paper is organized as follows: in Section II the problem is formulated, with the analytical auxiliary potentials given in Appendix A. In that appendix we also obtain analytically, with the help of the auxiliary potentials, the added-mass contributions to the lift and drag (or thrust) for any heaving motion of an elliptic airfoil at any mean angle of attack. These solutions also help to the validation of the numerical method, which is described in Section III, and validated further in Appendix B with results from previous works. The numerical results are presented and discussed in Section IV, and the main conclusions are summarized in Section V.

II. FORMULATION OF THE PROBLEM

We consider here the two-dimensional unsteady and incompressible flow of a uniform current over an oscillating ellipse. In particular, the ellipse, which represents a wing element with chord length c and thickness e, forms an angle α with the current of constant speed U (see Fig. 1) , and performs a sinusoidal heaving motion perpendicular to the current with amplitude h_0 and frequency f,

$$h(t) = h_0 \sin(2\pi f t)\,. \tag{1}$$

Using the chord c and the free stream speed U as the reference length and velocity, respectively, the non-dimensional Navier-Stokes equations and boundary conditions governing the incompressible flow can be written as

$$\nabla \cdot \mathbf{v} = 0\,, \tag{2}$$

$$\frac{\partial}{\partial t}\mathbf{v} + \mathbf{v}\cdot\nabla\mathbf{v} = -\nabla p + \frac{1}{Re}\nabla^2\mathbf{v}\,; \tag{3}$$

$$|\mathbf{x}| \to \infty\,, \quad \mathbf{v} \to \mathbf{e}_x\,, \quad p \to 0\,; \tag{4}$$

$$S(\mathbf{x},t) = 0\,, \quad \mathbf{v} = V_0(t)\mathbf{e}_y \equiv 2\pi St_a \cos(2\pi St_c t)\mathbf{e}_y\,, \tag{5}$$

where $\mathbf{v}$ is the non-dimensional velocity, p the non-dimensional relative pressure (scaled with ρU^2, being ρ the fluid density), $\mathbf{e}_x$ and $\mathbf{e}_y$ are the unit vectors in the direction of the free stream velocity and in its perpendicular direction, respectively, and $S(\mathbf{x},t) = 0$ defines the

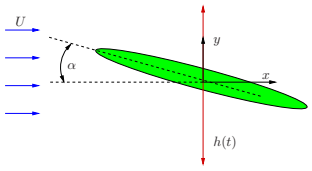

FIG. 1: Schematic of the problem.

non-dimensional position of the ellipse surface as a function of time in a fixed reference frame (see §III). In the above equations we have defined the following non-dimensional parameters:

$$Re = \frac{\rho U c}{\mu}\,, \quad St_a = \frac{h_0 f}{U}\,, \quad St_c = \frac{c f}{U}\,; \tag{6}$$

i.e., a Reynolds number based on the chord length c and two Strouhal numbers, one based on the amplitude of the oscillation h_0 and the other one on the chord length, being μ the fluid viscosity. These two Strouhal numbers are related to the advance ratio J and the reduced frequency k, respectively, usually defined in the flapping wing literature:[1,3]

$$J = \frac{U}{2\pi f h_0} = \frac{1}{2\pi St_a}\,, \quad k = \frac{2\pi f c}{U} = 2\pi St_c\,. \tag{7}$$

St_a is also related to the parameter kh used in Lewin and Haj-Hariri[38] by $kh = 2\pi St_a$.

The non-dimensional force (scaled with $\frac{1}{2}\rho U^2 c$) that the fluid exerts on the ellipse surface $S(\mathbf{x}, t) = 0$ can be written as the sum of the pressure and viscous friction forces,

$$\mathbf{F} = -2\int_S p\,\mathbf{n}\,ds + \frac{2}{Re}\int_S (\omega \wedge \mathbf{n})\,ds\,, \tag{8}$$

where $\mathbf{n}$ is the outward unit vector normal to the ellipse and $\omega = \nabla \wedge \mathbf{v}$ is the nondimensional vorticity field. The $x-$ and $y-$components of $\mathbf{F}$ are the drag and lift coefficients, respectively,

$$C_D = \mathbf{F}\cdot\mathbf{e}_x\,, \quad C_L = \mathbf{F}\cdot\mathbf{e}_y\,. \tag{9}$$

If $C_D < 0$ it becomes a *thrust* coefficient. Since we are using U as the reference velocity, the output or thrust power coefficient numerically coincides with $-C_D$, while the input power coefficient, or power needed to heave the airfoil, is the product of $-C_L$ and the heaving nondimensional velocity V_0 (5):

$$C_{Po} = -C_D\,, \quad C_{Pi} = -C_L V_0\,. \tag{10}$$

We shall compute these quantities both instantaneously and integrated over time to obtain the work done in propelling the airfoil, W_o, and the work needed to heave it, W_i. These integrals are made over a cycle or stroke of the airfoil, of duration St_c^{-1}. The ratio is the thrust efficiency,

$$\eta = \frac{W_o}{W_i}\,. \tag{11}$$

In the fully developed flow, these quantities may vary from cycle to cycle if the fluid motion does not become periodic with the same frequency as the heaving motion, and we shall define also average values over a number of strokes (see Section IV A).

Alternatively, we shall obtain the drag and the lift coefficients using a formulation developed by Chang[46] that allows for a quantitative identification of the contributions of the different vortex flow structures to these forces (see also Ref.[47,48]):

$$C_D = -2\int_S \bar{\phi}\frac{\partial \mathbf{v}}{\partial t}\cdot \mathbf{n} ds + \int_S v^2 \mathbf{n}\cdot\mathbf{e}_x ds - 2\int_V (\mathbf{v}\wedge\omega)\cdot\nabla\bar{\phi}\, dV + \frac{2}{Re}\int_S (\omega\wedge\mathbf{n})\cdot(\nabla\bar{\phi}+\mathbf{e}_x)\, ds$$
$$\equiv C_{Da} + C_{Dm} + C_{Dv} + C_{Ds}\,, \tag{12}$$

$$C_L = -2\int_S \phi\frac{\partial \mathbf{v}}{\partial t}\cdot \mathbf{n} ds + \int_S v^2 \mathbf{n}\cdot\mathbf{e}_y ds - 2\int_V (\mathbf{v}\wedge\omega)\cdot\nabla\phi\, dV + \frac{2}{Re}\int_S (\omega\wedge\mathbf{n})\cdot(\nabla\phi+\mathbf{e}_y)\, ds$$
$$\equiv C_{La} + C_{Lm} + C_{Lv} + C_{Ls}\,, \tag{13}$$

where V is the volume (area in our $2D$ case) limited by the ellipse surface (curve) S and the outer surface of the computational domain as $|\mathbf{x}|\to\infty$, while the auxiliary potential functions ϕ and $\bar{\phi}$ are given, respectively, by

$$\nabla^2\phi = 0 \quad \text{in}\, V\,, \tag{14}$$

$$|\mathbf{x}|\to\infty\,, \quad \phi\to 0\,, \quad \mathbf{n}\cdot\nabla\phi = -\mathbf{n}\cdot\mathbf{e}_y \quad \text{on}\, S\,, \tag{15}$$

and

$$\nabla^2\bar{\phi} = 0 \quad \text{in}\, V\,, \tag{16}$$

$$|\mathbf{x}|\to\infty\,, \quad \bar{\phi}\to 0\,, \quad \mathbf{n}\cdot\nabla\bar{\phi} = -\mathbf{n}\cdot\mathbf{e}_x \quad \text{on}\, S\,. \tag{17}$$

These functions ϕ and $\bar{\phi}$ are obtained analytically in Appendix A. Note that the friction force [second term in (8)] becomes a fraction of the surface integrals C_{Ds} and C_{Ls} in the drag and lift coefficients (12) and (13), while the other fraction of these surface integrals, together with the remaining components, come from the pressure force term in (8). The volume integrals C_{Dv} and C_{Lv} are of special interest here because their integrands may be interpreted as volumetric densities of the drag (or thrust) and the lift forces, respectively, identifying the relative contributions of the different vortices and other flow structures to the drag (or thrust) and lift forces on the flapping ellipse at each instant. In particular, we shall use the drag (or thrust) density δ_{Dv} (defined in §IV A) to characterize quantitatively the vortex structures contributing to the optimum thrust efficiency. Finally, it can be shown that the rotational components C_{Dm} and $C_{Lm} = 0$ vanish in the present problem, while the added mass components C_{Da} and C_{La} can be obtained analytically (see details in Appendix A).

III. NUMERICAL METHOD

We solve numerically (2)-(5) in a spatial grid around the ellipse which is obtained by a Joukowski transformation[49] that maps a circle of radius a centred at the origin into an ellipse with main axis of length unity forming and angle $-\alpha$ with the horizontal axis x (see Fig. 1), and minor axis length $\epsilon = e/c$. This transformation between the $\tau = \xi + i\eta$ complex plane of the circle and the $z = x + iy$ complex plane of the ellipse can be written as

$$z = \left(\tau + \frac{1-\epsilon^2}{16\tau}\right) e^{-i\alpha}\,, \tag{18}$$

with the radius of the circle given by $a = (1+\epsilon)/4$. The fixed ellipse with chord length 1 is obtained by the transformation of the circle $\tau = ae^{i\theta}$, for $0 \le \theta \le 2\pi$, and is given by $z = (\cos\theta + i\epsilon\sin\theta)e^{-i\alpha}$, or, in cartesian coordinates,

$$x = x_0(\theta) \equiv \frac{1}{2}\cos\alpha\cos\theta + \frac{\epsilon}{2}\sin\alpha\sin\theta\,, \tag{19}$$

$$y = y_0(\theta) \equiv -\frac{1}{2}\sin\alpha\cos\theta + \frac{\epsilon}{2}\cos\alpha\sin\theta\,, \quad 0 \le \theta \le 2\pi\,. \tag{20}$$

Thus, the flapping ellipse, denoted by $S(\mathbf{x}, t) = 0$ in (5), is given, in terms of the parameter θ, by

$$x = x_0(\theta)\,, \quad y = y_0(\theta) + H(t)\,, \quad H(t) = \frac{h_0}{c}\sin(2\pi St_c t)\,, \quad \frac{h_0}{c} = \frac{St_a}{St_c}\,. \tag{21}$$

The outer boundary of the computational domain, where the boundary conditions (4) are numerically imposed, is chosen as the transformation of the circle $\tau = R_o e^{i\theta}$, with $R_o \gg 1$, which is also 'almost' a circle in the plane z. As an illustration, Fig. 2 shows an example of a very coarse mesh in the plane τ and its transformation into the plane z for $R_o = 2.5$, $\epsilon = 1/8$ ($a = 9/32$) and $\alpha = 45^o$, with 128 nodal points on the circle (and ellipse) and a total of 10240 grid elements. In the reported computations we used finer meshes with much more elements and larger values of R_o (see convergence analysis in Appendix B).

Since the ellipse is moving with velocity $V_0\mathbf{e}_y$ given by (5), we used a moving and deforming mesh whose motion is prescribed by solving the Laplace equation $\nabla\cdot(k\nabla\mathbf{x}) = 0$, where $\mathbf{x}$ is the displacement field and k is a diffusion coefficient which is chosen to decrease quadratically with the distance l from the moving boundary, $k(l) = 1/l^2$ (see, e.g., Ref.[50] for details).

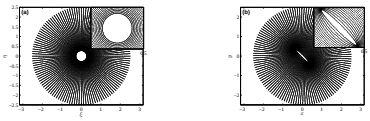

FIG. 2: Mesh example in the τ plane (a) and its transformation into the z plane (b). Details of the grids near the inner circle and the ellipse are given in the insets. $R = 2.5$, $\epsilon = 1/8$ and $\alpha = 45^o$.

To solve numerically equations (2)-(5) and (14)-(17) in the above described dynamic mesh we used the software OpenFOAM®, an open source Computational Fluid Dynamics (CFD) package based on the finite volume method. For the spatial discretization we used second order accuracy linear interpolation for the diffusion term, and a Total Variation Diminishing scheme, TVD, with a van Leer limiter, for the convection term. This hybrid scheme is set in order to avoid numerical oscillations in grid regions where local mesh Reynolds number is high (far field) and convection dominates over diffusion. On the other hand, the temporal discretization was performed by blending a second order Crank-Nicolson scheme with implicit Euler integration, to ensure boundedness of the solution. Moreover, the pressure-velocity coupling has been treated through the pressure-implicit split-operator (PISO) algorithm,[51] using a small temporal step to keep the maximum Courant number under 0.5. Finally,

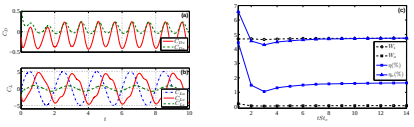

FIG. 3: Different components of C_D (a) and C_L (b) vs. t for $Re = 500$, $\alpha = 0$, $St_a = 0.16$ and $St_c = 0.5$. (c): Input and output works, W_i and W_o, and efficiencies η and η_v vs. the increasing number of strokes tSt_c for the same case.

the integrals to compute the different forces coefficients were discretized with second-order accuracy by using the midpoint rule in combination with linear interpolation schemes

We set an impulsively started flow past an ellipse located at the center of the domain as initial conditions. Validation with results from previous works and convergence analyses are given in Appendix B. In addition, a validation of the numerical results against analytical results for C_{La} and C_{Da} are given in Appendix A.

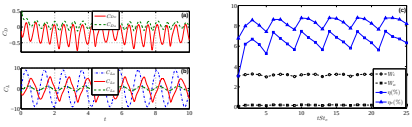

FIG. 4: As in Fig. 3, but for $St_c = 0.9$.

IV. RESULTS AND DISCUSSION

A. Flow characteristics for a fixed St_a and $\alpha = 0$

We consider first the case $St_a = 0.16$ (i.e., $J \simeq 1$) with detail to discuss the different flow structures as the heaving frequency (St_c) is varied, and their effect in the thrust power and efficiency. All the results are for $Re = 500$ and $\alpha = 0$.

Figures 3-4 show the evolution in time of the different components of C_D and C_L as well as the output (thrust) and input works and efficiencies as functions of the successive strokes ($n = tSt_c$) for two frequencies: $St_c = 0.5$ and $St_c = 0.9$. Note that $C_{Da} = 0$ for $\alpha = 0$ (see Appendix A), that is corroborated numerically with the computed auxiliary potential $\bar{\phi}$. The 'volumetric' efficiency is defined as $\eta_v = W_{ov}/W_i$ [compare with (11)], where

$W_o = W_{ov} + W_{os}$, with W_{ov} and W_{os} computed integrating $-C_{Dv}$ and $-C_{Ds}$, respectively, over a period of one stroke $T = St_c^{-1}$. We can also define a 'surface' efficiency $\eta_s = W_{os}/W_i$, but it is not necessary because $\eta_v + \eta_s = \eta$.

For the first frequency (Fig. 3) the flow becomes periodic and, therefore, the different works and efficiencies, which are integrated over a stroke, tend to constant values. However, Fig. 4(a) shows that for the higher frequency $St_c = 0.9$ the flow never reaches a periodic state with the heaving frequency, so that the works and efficiencies never tend to constant values. In this particular case, the flow is not completely *aperiodic*: Figure 4(c) shows that the flow reaches a quasi-periodic state, with a period of four full strokes of the airfoil.

To analyze the main differences in the flow structure, we note first that C_{La} is always in phase and proportional to the airfoil heaving motion (in fact it is proportional to the vertical acceleration, as obtained analytically in Appendix A):

$$C_{La} = 2\pi^3 St_c St_a \sin(2\pi St_c t) = 2\pi^3 St_c^2 H(t)\,. \tag{22}$$

This expression corresponds to the added mass contribution to the lift, and it is corroborated by using the auxiliary potential ϕ obtained numerically from (14)-(15) (see Appendix A; in fact, all the reported results are obtained numerically, not using (22) nor any of the other analytical expressions given in Appendix A). Thus, this term helps to compare the temporal oscillations of the other components of C_L and C_D with the airfoil oscillations in Figs. 3-4 and subsequent similar figures. Note that (22) is valid for any horizontal ellipse moving harmonically in the vertical direction, independently of its thickness ϵ.

The oscillations of the two components of C_D [Figs. 3(a) and 4(a)] have a frequency twice that of the heaving motion due to the vortex formation and shedding during each half stroke (see below), while the oscillations of the other two components of C_L have the same frequency as the heaving motion, but both with a substantial phase shift. However, in the case of $St_c = 0.9$, these oscillations are not periodic like in the case of $St_c = 0.5$, as already commented. It is also observed in Figs. 3(a) and 4(a) that C_{Ds} is mostly positive, contributing to the drag, while C_{Dv} is mostly negative, contributing to the thrust of the airfoil. But the overall effect is a net thrust because the mean contribution of C_{Dv} is larger than that of C_{Ds} in both cases. This is clearly seen in the positive values of W_o and η in both cases [Figs. 3(c) and 4(c)], and in the fact that the volumetric efficiency η_v is also

larger than the total efficiency η in both cases (this means that η_s is obviously negative).

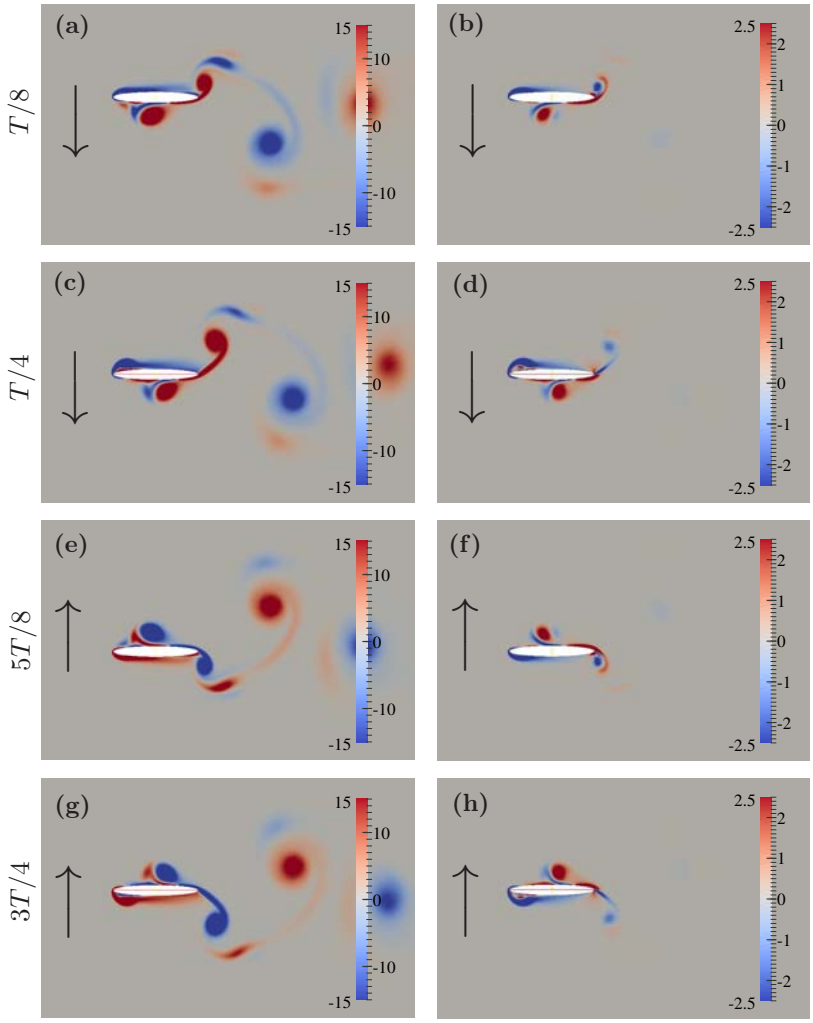

FIG. 5: Snapshots of ω (left panels) and of δ_{Dv} (right panels) at several significative instants of time within the same stroke ($T = St_c^{-1}$ denotes the non-dimensional period of one stroke, starting from the beginning of the downstroke) for $St_a = 0.16$, $St_c = 0.5$, $Re = 500$ and $\alpha = 0$. (Multimedia view: video 1)

To explain these results in terms of the flow structure we plot in Figs. 5-6 the vorticity fields at several instants of time for these two values of St_c, together with the corresponding 'drag density' (δ_{Dv}) fields. This density is defined as the integrand of C_{Dv} in (12):

$$C_{Dv} = \int_V \delta_{Dv}\, dV\,, \qquad \delta_{Dv} \equiv 2(\omega \wedge \mathbf{v}) \cdot \nabla \bar{\phi}\,; \tag{23}$$

δ_{Dv} is negative in the points where the flow contribute to the thrust of the airfoil, and positive in the points that contribute to the drag. Note that δ_{Dv} is twice the projection

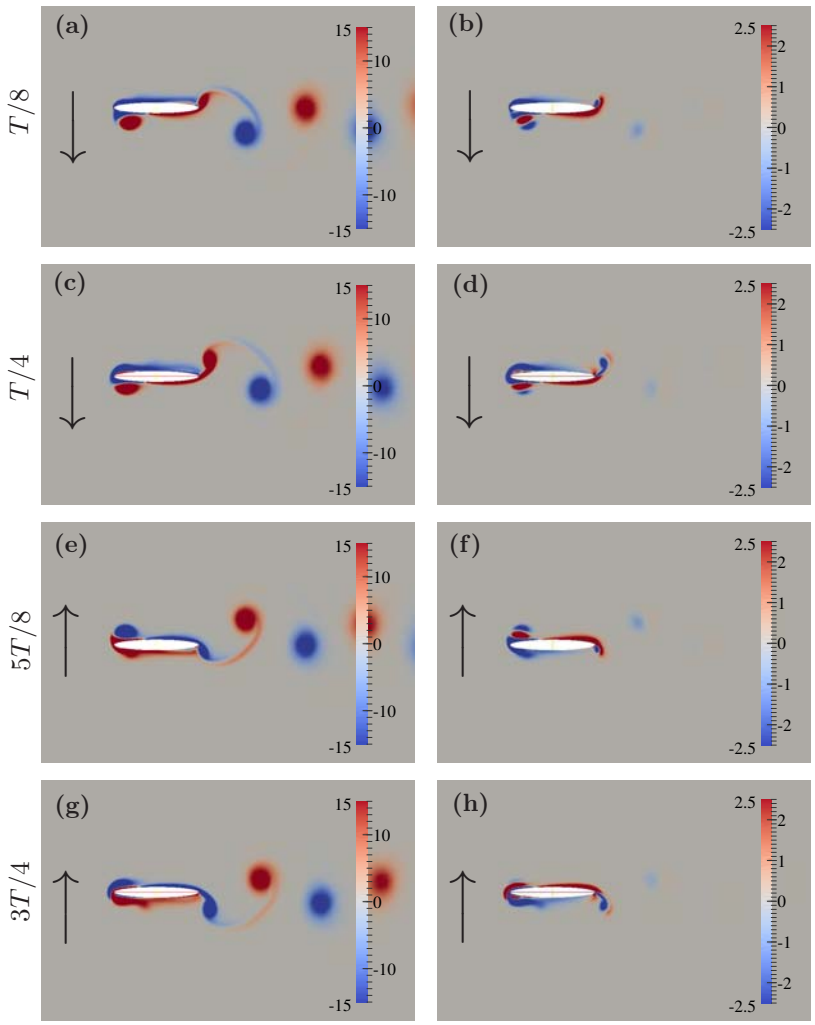

FIG. 6: Snapshots of ω (left panels) and of δ_{Dv} (right panels) at several significative instants of time within the same stroke for $St_a = 0.16$, $St_c = 0.9$, $Re = 500$ and $\alpha = 0$. (Multimedia view: video 2)

of Lamb's vector $\omega \wedge \mathbf{v}$, responsible for this vortex force,[52] on the gradient of the auxiliary potential $\bar{\phi}$. This ensures that δ_{Dv} decays fast as we move away from the airfoil, because, according to (16)-(17), far from the (moving) 2D body $\nabla\bar{\phi}$ decays quadratically with the distance to it.[53] Note that in the present 2D flow, δ_{Dv} can be written as

$$\delta_{Dv} = -2\omega v\frac{\partial\bar{\phi}}{\partial x} + 2\omega u\frac{\partial\bar{\phi}}{\partial y}\,, \tag{24}$$

where $\mathbf{v} = u\mathbf{e}_x + v\mathbf{e}_y$ and $\omega = \omega\mathbf{e}_z$ (this z-component of the vorticity is the quantity plotted in the left panels of Figs. 5-6).

We observe in Fig. 5 ($St_c = 0.5$) that thrust is generated (δ_{Dv} is negative) during the

formation of the leading-edge vortex (LEV), especially in the first part of each downstroke [Figs. 5(a)-(d)] and each upstroke [Figs. 5(e)-(h)], and by the shedding trailing-edge vortex (TEV) of the previous half stroke. Drag is generated (positive δ_{Dv}) during the formation of the TEV, especially in the first part of each downstroke and each upstroke, and by the shedding LEV of the previous half stroke when captured and stretched by the current half stroke.

The main difference of the case $St_c = 0.9$ (Fig. 6) is that most of the LEV generated in each half stroke is not shed for this higher frequency. A significant fraction of the LEV remains at the leading edge (LE), stretching and diffusing during the subsequent half strokes, thus generating significantly less drag. Since the other thrust and drag generating episodes remains practically the same, the total thrust work and efficiency are larger for this higher frequency than for $St_c = 0.5$ [compare Figs. 3(c) and 4(c)]. A fraction of each LEV vorticity that is not diffused is eventually shed, joining the TEV of the corresponding half stroke. This happens every four strokes in this case (see multimedia view corresponding to Fig. 6), explaining the periodicity of four strokes in Fig. 4(c).

Note that in both cases a thrust-producing reverse-Kármán-vortex-street wake is generated, as it was characterized experimentally by Jones et al.[30] and by Lai and Platzer.[31] To the generation of these vortices in the wake contributes both the LEVs and the TEVs, as previously found numerically by Lewin and Haj-Hariri,[38] and observed experimentally by Lua et al.,[43] also for a heaving, two-dimensional elliptic airfoil.

Figure 7 shows the mean values of the input and output works and efficiencies, $\bar{W}_o, \bar{W}_i, \bar{\eta}$ and $\bar{\eta}_v$, as functions of the frequency St_c for the present case $St_a = 0.16$. For the frequencies where the flow becomes periodic with the heaving frequency, these mean values correspond to the asymptotic constant values of W_o, W_i, η and η_v, respectively [e.g., Fig. 3(c)]. For the remaining frequencies we average these quantities over a sufficiently large number of strokes to get a mean value with an error less that 2.5% (see §IV B). The oscillations in these quantities are characterized by their standard deviations with error bars in Fig. 7. It is observed that, in the present case $St_a = 0.16$, the flow does not become periodic with the frequency of the heaving motion only for $St_c = 0.9$ and 1.1. For these two frequencies the flow is not aperiodic (chaotic), as it happens for larger St_a (see below), but acquires a periodicity of several strokes (4 and 3, respectively). Therefore, averaging over these numbers of cycles is enough to obtain accurately the mean values given in Fig. 7. More

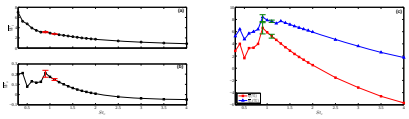

FIG. 7: Mean values of W_i (a), W_o (b), η and η_v (c) as functions of St_c for $St_a = 0.16$, $Re = 500$ and $\alpha = 0$.

complex aperiodic motions will be described in the following sections.

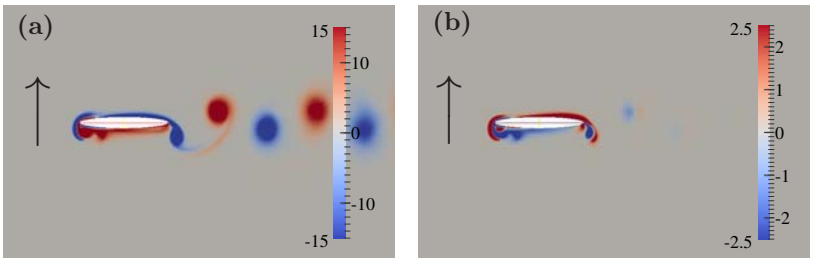

FIG. 8: Snapshots of ω (a) and of δ_{Dv} (b) at the instant $3T/4$ within a stroke for $St_a = 0.16$, $St_c = 1.2$, $Re = 500$ and $\alpha = 0$. (Multimedia view: video 3)

According to Fig. 7, the two frequencies analyzed above correspond to the maximum efficiency ($St_c = 0.9$) and to a local minimum ($St_c = 0.5$). As St_c augments from 0.9,

an increasing portion of the LEV generated in a previous half stroke moves around the LE to the other part of the airfoil [see Fig. 8 for $St_c = 1.2$ and compare with 6(g)-(h)], generating more drag, and thus reducing the total thrust and mean efficiency in relation to $St_c = 0.9$. Although the mean 'volumetric' efficiency $\bar{\eta}_v$ never becomes negative as St_c increases [see Fig. 7(c)], i.e., the regions with negative δ_{Dv} always weight more than the regions with positive δ_{Dv}, the global efficiency $\bar{\eta}$ becomes negative for $St_c \gtrsim 2$ due to the surface contribution C_{Ds}, which always contributes with a positive mean value (i.e., to the drag).

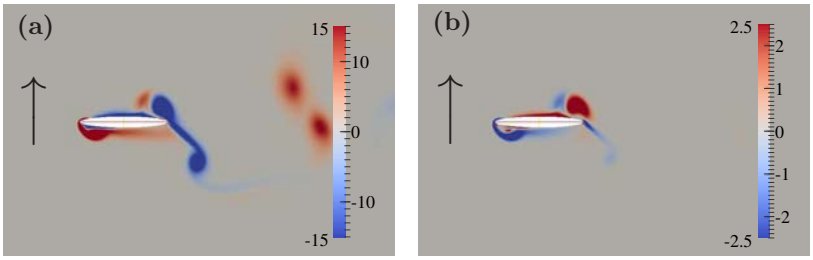

FIG. 9: Snapshots of ω (a) and of δ_{Dv} (b) at the instant $3T/4$ within a stroke for $St_a = 0.16$, $St_c = 0.4$, $Re = 500$ and $\alpha = 0$. (Multimedia view: video 4)

For $St_c = 0.4$ the efficiency presents a local maximum. The main difference with the case $St_c = 0.5$ is that the LEV of each previous half stroke when $St_c = 0.4$ is shed out from the airfoil before the end of the current half stroke (at $3T/8$ and $9T/8$, approximately), thus generating drag during less time [see Fig. 9 and compare with Fig. 5(g)-(h)]; i.e., the shedding LEV does not generate drag during the full second half of each half stroke, because in the final part it is too far from the airfoil. The other contributions remaining similar, this difference yields a larger output thrust and efficiency than for $St_c = 0.5$. For $0.5 < St_c < 0.9$, the flow is very similar to that for $St_c = 0.5$, and $\bar{W}_o$ remains almost constant. However, $\bar{\eta}$ increases with St_c because the input work $\bar{W}_i$ decreases with St_c (see Fig. 7). When St_c reaches the value 0.9, approximately, the LEV remains attached to the LE, it is no longer completely shed during each stroke and the total thrust increases, as already explained above. The mean thrust efficiency reaches a maximum at this frequency.

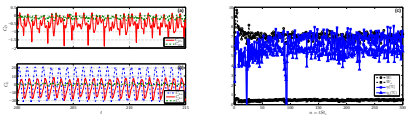

FIG. 10: Different components of C_D (a) and C_L (b) vs. t (only the last time interval computed is shown) for $Re = 500$, $\alpha = 0$, $St_a = 0.24$ and $St_c = 1.4$. (c): Input and output works, W_i and W_o, and efficiencies η and η_v vs. the increasing number of cycles n for the same case.

B. Thrust efficiency for $\alpha = 0$

We summarize here the results for several values of St_a ranging from 0.12 to 0.24 (i.e., for $1.35 \gtrsim J \gtrsim 0.66$) when $\alpha = 0$ and $Re = 500$. As commented on above, in the case that the flow does not become periodic with the same frequency as the heaving motion, we average the integrated works W_i and W_o and the corresponding efficiencies over a sufficiently large number of cycles n such that the relative error in the mean efficiency $\bar{\eta}$ is smaller than 2.5%. For strongly aperiodic flows the number of cycles n needed may be quite large. For this reason, when the flow is aperiodic, we first average over 300 cycles and check than the relative error is less than 2.5%. For instance, for $St_a = 0.24$ and $St_c = 1.4$ (Fig. 10), this

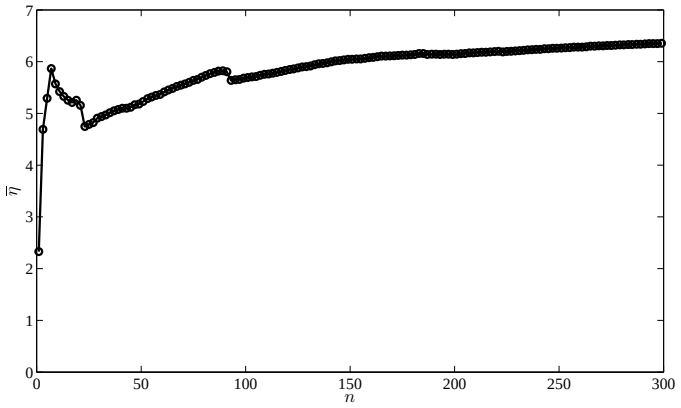

FIG. 11: Average value of the efficiency $\bar{\eta}$ as a function of the number of cycles used for computing the mean. $St_a = 0.24$, $St_c = 1.4$, $Re = 500$, $\alpha = 0$.

criterium is satisfied with $n = 300$ (Fig. 11). If it is not so, we use larger values of n until the criterium is met, but that happens only for a few number of cases among those reported here.

Figures 12-13 show $\bar{W}_o, \bar{W}_i, \bar{\eta}$ and $\bar{\eta}_v$, as functions of the frequency St_c for the four values of St_a considered. For the sake of clarity of the figures we omit the errors bars that characterize the standard deviations of the mean values when the flow is not periodic with the heaving frequency (the standard deviations are given later together with a discussion on the periodic or aperiodic character of the flow in the different cases). $\bar{W}_i$ increases with St_a for a given St_c, and so does $\bar{W}_o$. The qualitative behavior of these average works with St_c is quite similar for all St_a. Since $\bar{W}_o$ has a pronounced maximum when St_c is near unity for all St_a for which $\bar{W}_o$ is positive (as already explained for $St_a = 0.16$ in the above section), the maximum efficiency is reached when St_c is close to unity, and for a value of St_a around 0.2. More concretely, among all the cased computed here, the maximum efficiency ($\bar{\eta}_{max} \simeq 9.3\%$) is reached for $St_c = 0.8$ when $St_a = 0.2$ [Fig. 13(a)], which corresponds to a reduced frequency of $k \simeq 5$ and an advance ratio $J \simeq 0.8$. These values for optimal thrust in forward flight of a horizontal 2D heaving wing are in agreement with previous experimental and numerical works for different airfoil geometries and Reynolds numbers[29,33–35,38,40,54] (note that the Strouhal number St used in some of the cited experimental works is $St = 2St_a$). In particular, Lewin and Haj-Hariri,[38] who used a different (more efficient) airfoil profile for the same Reynolds number, found that the maximum efficiency (of about 11%) is reached

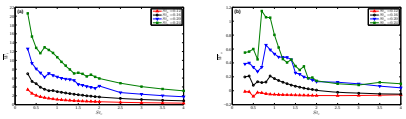

FIG. 12: $\bar{W}_i$ and $\bar{W}_o$ vs. St_c for the four values of St_a considered. $Re = 500$ and $\alpha = 0$.

at practically the same frequency and amplitude: $St_c \simeq 0.85$ and $St_a \simeq 0.19$.

For a better characterization of the optimum values of the heaving frequency and amplitude that generate the maximum average thrust efficiency, we plot in Fig. 14 the contours of constant $\bar{\eta}$ and constant $\bar{\eta}_v$ in the plane (St_a, St_c) using linear interpolation of the numerical data contained in Fig. 13. It is observed that $\bar{\eta}$ is larger than 8.8% (top contour line in Fig. 14) in a region $0.79 \leq St_c \leq 0.9$ and $0.19 \leq St_a \leq 0.22$, approximately, with the maximum value very close to the case $St_c = 0.8$ and $St_a = 0.2$ already commented on. This maximum of $\bar{\eta}$ corresponds to a flow that eventually becomes periodic with the heaving frequency, so that $\bar{\eta} = \eta$. But the flow is aperiodic for larger heaving frequencies when $St_a = 0.2$: As characterized in Fig. 15 by error bars, the flow is no longer periodic for $St_c \gtrsim 1.5$. To illustrate this, Fig. 16 compares the efficiency η as a function of the number of cycles $n = St_c t$ for the frequencies $St_c = 0.8$, $St_c = 1.5$ and $St_c = 2$, the first one corresponding to a periodic

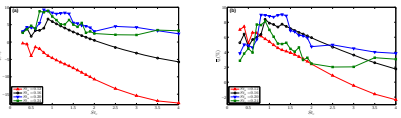

FIG. 13: $\bar{\eta}$ and $\bar{\eta}_v$ vs. St_c for the four values of St_a considered. $Re = 500$ and $\alpha = 0$.

flow (actually, the most thrust efficient one), the second one to an aperiodic flow, and the third one to a quasiperiodic flow. As noted by Blondeaux et al.,[42] very long simulations are needed in some cases to observe the chaotic flow, for sometimes it is preceded by a long quasi-periodic flow. These different behaviors are better identified by using phase diagrams of, for instance, C_L vs. C_D, for the fully developed flow [see Figs. 16(d)-(f)]. A limit cycle is reached for periodic and quasi-periodic flows, with several frequencies in the later case, while the phase diagram is chaotic for aperiodic flows (for the sake of clarity only a few cycles are plotted in this later case).

The flow for the optimum case $St_c = 0.8$ with $St_a = 0.20$ is quite similar to that described in Fig. 6 for the optimum case $St_c = 0.9$ when $St_a = 0.16$. The main qualitative difference is that now ($St_a = 0.20$) the flow is periodic with the heaving frequency, while for $St_a = 0.16$ the flow became periodic with a frequency four times smaller than the heaving frequency.

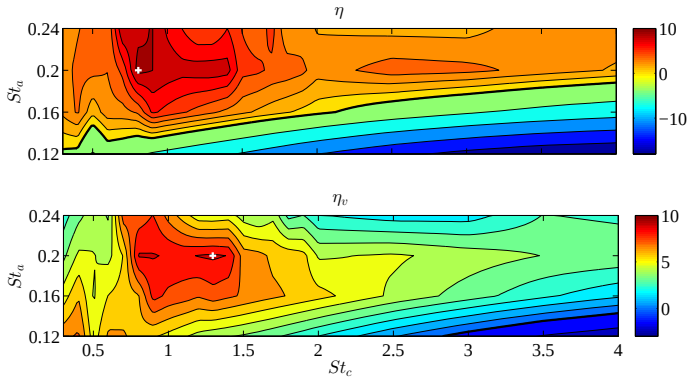

FIG. 14: Contour plot of $\bar{\eta}$ (top) and $\bar{\eta}_v$ in the (St_c, St_a)-plane. $Re = 500$ and $\alpha = 0$. The thick lines separate positive from negative values and the white crosses mark the locations of the maximum values.

But both share the main characteristic that most part of the LEV generated in each half stroke remains attached near the leading edge during the subsequent half strokes, where it is stretched and diffused, so that a region of positive thrust ($\delta_{Dv} < 0$) is always present around the LE, maximizing the thrust efficiency. In the present case, a small fraction of the LEV generated in any half stroke, which is stretched during the next one, split and move around the LE, being shed during the following half stroke on the opposite airfoil surface. Then, joins and reinforces the TEV (of the same sign) corresponding to that half stroke (see Fig. 17). Since this process repeats every cycle the flow is periodic with the heaving frequency.

However, for the higher frequency $St_c = 1.5$ (Fig. 18), a large fraction of the LEV generated in a previous half stroke moves around the LE to the other part of the airfoil, as in Fig. 8 for $St_c = 1.2$ and $St_a = 0.16$, generating more drag and reducing the total thrust and mean efficiency in relation to $St_c = 0.8$. But now, with the higher amplitude and frequency of the oscillations, a given LEV is split several times in successive half strokes, each fraction being convected downstream along one of the airfoil surfaces. Since these LEV portions are not always of the same size in successive strokes, and due also to their interactions with TEVs of equal and opposite sign, the flow becomes chaotic [Fig. 16(e)] and the efficiency aperiodic [Fig. 16(b)]. This transition from periodic to chaotic behaviors for sufficiently high frequencies and amplitudes has been documented for the 2D flow over a plunging airfoil at low Re by several authors for different airfoil geometries and Reynolds

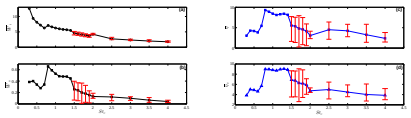

FIG. 15: $\bar{W}_i$ (a), $\bar{W}_o$ (b), $\bar{\eta}$ (c), and $\bar{\eta}_v$ as functions of St_c for $St_a = 0.20$, $Re = 500$ and $\alpha = 0$. The errors bars characterize the standard deviations of the mean values when the flow is not periodic with the heaving frequency.

numbers.[34,38,42,44,45] Three-dimensional numerical simulations by Ashraf et al.[55] of the flow over a plunging NACA0012 airfoil at a higher Re confirmed the chaotic behavior of forces with the increase in plunging amplitude found from 2D analysis at the same Re.

To finish this section, we characterize in a single plot (Fig. 19) the type of flow for the different values St_c and St_a when $\alpha = 0$ by the standard deviation of the oscillations in η. This quantity is obviously zero when the flow is periodic with the heaving frequency (marked with P in the figure), and different from zero both for aperiodic flows (AP), or for periodic flows with a different frequency (PO).

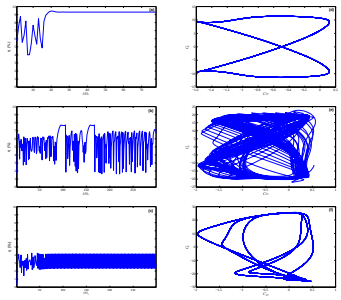

FIG. 16: (a)-(c) η vs. $n = tSt_c$, (d)-(f) phase diagrams of C_L vs. C_D, for $St_a = 0.20$, $Re = 500$, $\alpha = 0$, and $St_c = 0.8$ [(a) and (d)], $St_c = 1.5$ [(b) and (e)], $St_c = 2$ [(c) and (f)].

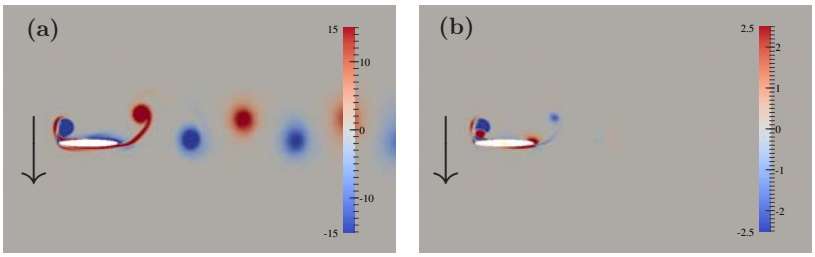

FIG. 17: Snapshots of ω (a) and of δ_{Dv} (b) at the instant $T/2$ within a stroke for $St_a = 0.20$, $St_c = 0.8$, $Re = 500$ and $\alpha = 0$. (Multimedia view: video 5)

C. Thrust efficiency for $\alpha \neq 0$

To analyze the effect that a mean angle of attack α different from zero has on the vortex structure of the flow and, consequently, on the thrust efficiency, we consider in this section several cases for St_c and St_a close to their values of maximum efficiency when $\alpha = 0$. Since

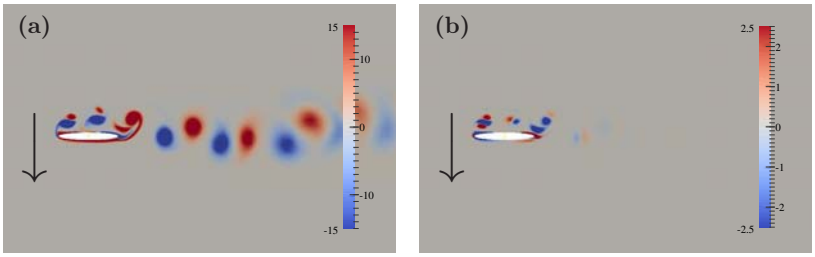

FIG. 18: Snapshots of ω (a) and of δ_{Dv} (b) at the instant $T/2$ within a stroke for $St_a = 0.20$, $St_c = 1.5$, $Re = 500$ and $\alpha = 0$. (Multimedia view: video 6)

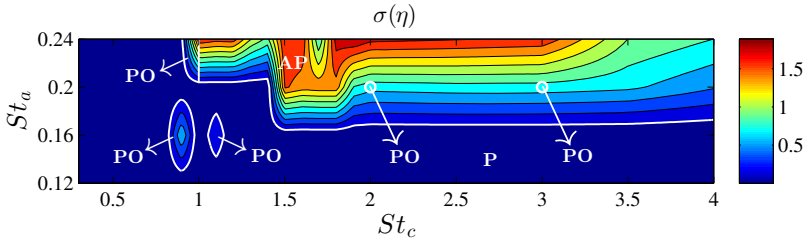

FIG. 19: Contour plot of the standard deviation of η (top) and η_v (bottom) in the (St_c, St_a)-plane. $Re = 500$ and $\alpha = 0$. The thick lines separate the regions with a periodic flow with the heaving frequency (P), the regions with aperiodic flows (AP), and the regions with periodic flows but with different frequencies (PO).

the problem is symmetric with respect to $\alpha = 0$, only values $\alpha \leq 0$ are considered.

Figure 20 shows the results as α varies from -10^o to 0^o for the case $St_a = 0.20$, and $St_c = 0.8$, the most thrust efficient one when $\alpha = 0$. It is observed that the largest mean efficiency $\bar{\eta}$ remains for $\alpha = 0$, and that the flow is no longer periodic with the heaving frequency even for small $|\alpha|$. In particular, the flow becomes aperiodic for $\alpha = -2.5^o$. This is because, compared to the flow with $\alpha = 0^o$ (Fig. 17), the trajectories of the split fractions of the LEV that move around the LE and are shed on the opposite airfoil surfaces depend on whether the LEV was generated during the up- or the down-stroke. This up-down asymmetry generates a deflected wake and an aperiodic flow (see Fig. 21). The flow remains aperiodic as $|\alpha|$ increases, becoming quasi-periodic, or periodic with a different frequency, for $|\alpha| = 7.5^o$, and periodic again for $|\alpha| = 10^o$ (this is marked in Fig. 20 with different symbols).

We have repeated the computations as $|\alpha|$ increases for several values of St_a and St_c. The results are summarized in Figs. 22-24. The trends are quite similar to the case com-

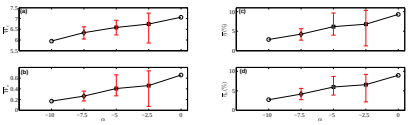

FIG. 20: $\bar{W}_i$ (a), $\bar{W}_o$ (b), $\bar{\eta}$ (c), and $\bar{\eta}_v$ as functions of α (in degrees) for $St_a = 0.20$, $St_c = 0.8$, $Re = 500$. Circles correspond to periodic flows with the heaving frequency. The errors bars characterize the standard deviations of the mean values when the flow is not periodic with the heaving frequency (squares correspond to aperiodic flows and diamonds to quasi-periodic flows).

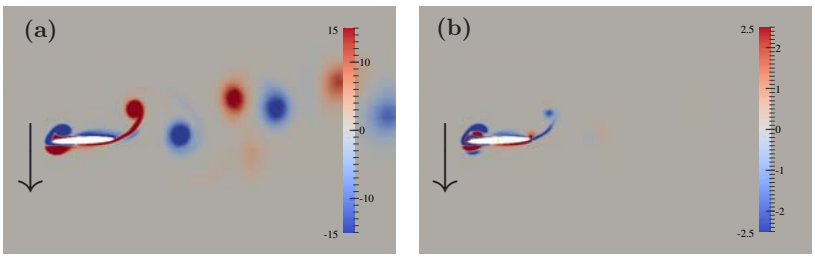

FIG. 21: Snapshots of ω (a) and of δ_{Dv} (b) at the instant $T/2$ within a stroke for $St_a = 0.20$, $St_c = 0.8$, $Re = 500$ and $\alpha = -2.5^o$. (Multimedia view: video 7)

mented on above, with periodic flows for $\alpha = 0$ in the cases of interest (maximum averaged

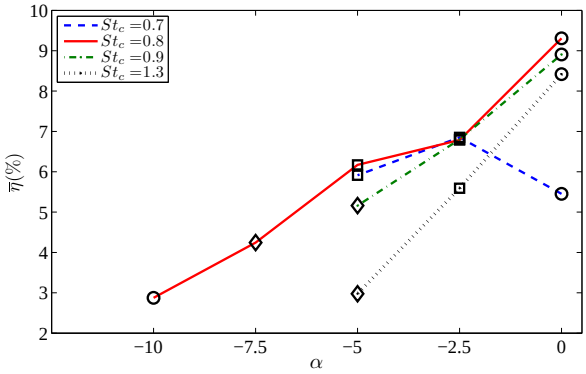

FIG. 22: $\bar{\eta}$ vs. α (in degrees) for $St_a = 0.20$, $Re = 500$ and different values of St_c (as indicated). Circles correspond to periodic flows with the heaving frequency, squares to aperiodic flows and diamonds to quasi-periodic or periodic flows with a different frequency (the errors bars characterizing the standard deviations of the mean values are not shown for simplicity).

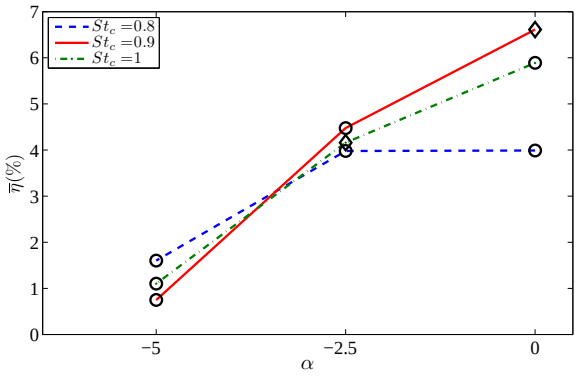

FIG. 23: As in Fig. 22, but for $St_a = 0.16$.

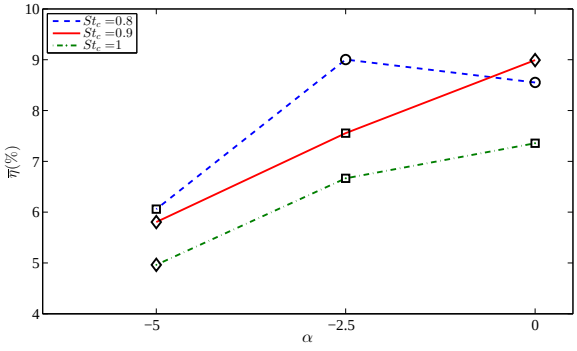

FIG. 24: As in Fig. 22, but for $St_a = 0.24$.

thrust efficiency), aperiodic for small $|\alpha|$, becoming quasi-periodic, and periodic again as $|\alpha|$ increases in most cases. Also, for most St_a and St_c, the maximum $\bar{\eta}$ takes place at $\alpha = 0$. The situation is more irregular for the largest heaving amplitude considered ($St_a = 0.24$, Fig. 24), where the flow may become aperiodic or quasi-periodic for $\alpha = 0$, or periodic for $|\alpha|$ small, depending on the value of St_c. Finally, it is noteworthy that the most thrust efficient configuration among all the cases considered corresponds to $\alpha = 0$ when $St_a = 0.2$ and $St_c = 0.8$, a case described with detail in the previous section.

V. CONCLUSION

We have conducted 2D numerical simulations of the flow around a heaving elliptic airfoil for different values of the mean angle of attack α, amplitude and frequency of the heaving motion, St_a and St_c, and for a given low Reynolds number ($Re = 500$) of interest in MAV and insect flapping flight. The vortex force decomposition used in this work yields analytic expressions for added-mass contributions to the lift and drag force components for any heaving motion of the elliptic airfoil for any α. This circumstance permits an additional validation of the numerical code. More importantly, the vortex force formulation allows for a quantitative characterization of the thrust (or drag) and lift force components exerted by any particular vortex structure of the flow on the airfoil. Basically, we find that thrust is mainly generated by the growing leading-edge vortex (LEV) during the initial part of each half stroke, and by the shedding trailing-edge vortex (TEV) of the previous half stroke when it is still near the airfoil. On the other hand, drag is mainly generated by the growing TEV during the initial part of each half stroke, and by the shedding LEV of the previous half strokes (depending on the frequency and amplitude, St_c and St_a) when stretched by the current half stroke. Using these mechanisms, we explain quantitatively the configurations of maximum thrust efficiency in terms of vortex flow structure and interaction. We find that, for the present heaving elliptic airfoil at $Re = 500$, the maximum thrust efficiency is reached for $St_a \simeq 0.2$ and $St_c \simeq 0.8$ with $\alpha = 0$. This configuration corresponds to a periodic flow with the heaving frequency. As another interesting result we find that as $|\alpha|$ increases slightly from zero this thrust efficient flow becomes aperiodic and the average thrust efficiency decreases.

It must be emphasized, to finish, that we have selected a simple 2-D flow around an

elliptic airfoil because it allows a much more detailed quantitative study of the different flow structures contributing to the thrust generation and to the propulsive efficiency using a vortex force decomposition analysis. The present work is focused to shed further light on the interesting fluid physics involved in these processes in a simple plunging airfoil at different mean angles of attack. Of course, the formalism of Chang for the evaluation of the force on the airfoil can be applied to three dimensional flows, flexible wing structures, and complex flapping kinematics, effects omitted in the present study but that play major roles in determining flapping wing aerodynamics.[1,56–61]

APPENDIX A: AUXILIARY POTENTIALS AND ANALYTICAL EXPRESSIONS FOR C_{Da} AND C_{La}

In the case of an elliptic surface S, Laplace equation in (14)-(17) can be solved analytically by separation of variables using elliptic coordinates,[62] in a reference frame moving with the ellipse. For an ellipse with its main axis of length unity in the x-axis (i.e., $\alpha = 0$), the elliptic coordinates (ξ, η) are related to (x, y) through

$$x = \frac{1}{2}\sqrt{1-\epsilon^2}\cosh\xi\cos\eta\,, \quad y = \frac{1}{2}\sqrt{1-\epsilon^2}\sinh\xi\sin\eta\,, \tag{A1}$$

where ϵ is the minor axis length in the y-axis, and the ellipse S is given by $\xi = \xi_0 = \ln[(1+\epsilon)/(1-\epsilon)]/2$, and $0 \leq \eta \leq 2\pi$. In these coordinates, the solutions to the problems (14)-(15) and (16)-(17) can be written, respectively,

$$\phi = \frac{1}{2}\sqrt{\frac{1+\epsilon}{1-\epsilon}}e^{-\xi}\sin\eta\,, \quad \bar{\phi} = \frac{\epsilon}{2}\sqrt{\frac{1+\epsilon}{1-\epsilon}}e^{-\xi}\cos\eta\,, \tag{A2}$$

which on the ellipse are

$$\phi = \phi_0 = \frac{1}{2}\sin\eta\,, \quad \bar{\phi} = \bar{\phi}_0 = \frac{\epsilon}{2}\cos\eta\,. \tag{A3}$$

For an ellipse at an angle $-\alpha$ with the x-axis, like in Fig. II, one only has to *rotate* the coordinate axes in the boundary conditions (15) and (17) on the surface of the ellipse, to get

$$\phi = \frac{1}{2}\sqrt{\frac{1+\epsilon}{1-\epsilon}}e^{-\xi}(\cos\alpha\sin\eta - \epsilon\sin\alpha\cos\eta)\,, \quad \bar{\phi} = \frac{1}{2}\sqrt{\frac{1+\epsilon}{1-\epsilon}}e^{-\xi}(\sin\alpha\sin\eta + \epsilon\cos\alpha\cos\eta)\,, \tag{A4}$$

$$\phi_0 = \frac{1}{2}(\cos\alpha\sin\eta - \epsilon\sin\alpha\cos\eta)\,, \quad \bar{\phi}_0 = \frac{1}{2}(\sin\alpha\sin\eta + \epsilon\cos\alpha\cos\eta)\,, \tag{A5}$$

where (ξ, η) are the elliptic coordinates on the 'rotated' ellipse.

For any surface S moving with a velocity $\mathbf{V}$ that does not vary along the surface (it may depend on time like in the present sinusoidal heaving motion), the 'm' (or rotational) components of C_D and C_L in (12) and (13) vanish:

$$C_{Dm} = \oint_S v^2 \mathbf{n}\cdot\mathbf{e}_x ds = V^2(t)\oint_S \mathbf{n}\cdot\mathbf{e}_x ds = 0\,, \tag{A6}$$

and similarly for C_{Lm}, where the circle in the integral symbol has been included to emphasize that S is a closed surface. On the other hand, the 'a' components in the case of an ellipse can be obtained analytically using the auxiliary potentials (A5) on the ellipse:

$$C_{Da} = -2\int_S \bar{\phi}\frac{\partial \mathbf{v}}{\partial t}\cdot\mathbf{n}ds = -2\frac{d\mathbf{V}}{dt}\cdot\int_0^{2\pi}\bar{\phi}_0\mathbf{e}_\xi h_\eta d\eta =$$
$$= -\frac{\pi}{2}\left[(1-\epsilon^2)\sin\alpha\cos\alpha\frac{dV_y}{dt} + (\sin^2\alpha + \epsilon^2\cos^2\alpha)\frac{dV_x}{dt}\right]\,, \tag{A7}$$

where use has been made of $\mathbf{n} = \mathbf{e}_\xi = \sqrt{1-\epsilon^2}(\sinh\xi_0\cos\eta\,\mathbf{i} + \cosh\xi_0\sin\eta\,\mathbf{j})/(2h_\xi)$ over the ellipse $\xi = \xi_0$, with $\mathbf{i}$ and $\mathbf{j}$ the unit vectors along the axes of the ellipse, and $h_\eta = h_\xi$. Note that the components of $\mathbf{V}$ on the (x, y) axes have been projected on $\mathbf{i}$ and $\mathbf{j}$. Similarly for C_{La}:

$$C_{La} = -2\int_S \phi\frac{\partial \mathbf{v}}{\partial t}\cdot\mathbf{n}ds = -2\frac{d\mathbf{V}}{dt}\cdot\int_0^{2\pi}\phi_0\mathbf{e}_\xi h_\eta d\eta =$$
$$= -\frac{\pi}{2}\left[(\cos^2\alpha + \epsilon^2\sin^2\alpha)\frac{dV_y}{dt} + (1-\epsilon^2)\sin\alpha\cos\alpha\frac{dV_x}{dt}\right]\,. \tag{A8}$$

Clearly these are *added-mass* terms of the hydrodynamic forces.[63]

In the present vertical heaving motion ($V_x = 0$), one has

$$C_{Da} = -\frac{\pi}{2}(1-\epsilon^2)\sin\alpha\cos\alpha\frac{dV_y}{dt}\,, \quad C_{La} = -\frac{\pi}{2}(\cos^2\alpha + \epsilon^2\sin^2\alpha)\frac{dV_y}{dt}\,, \tag{A9}$$

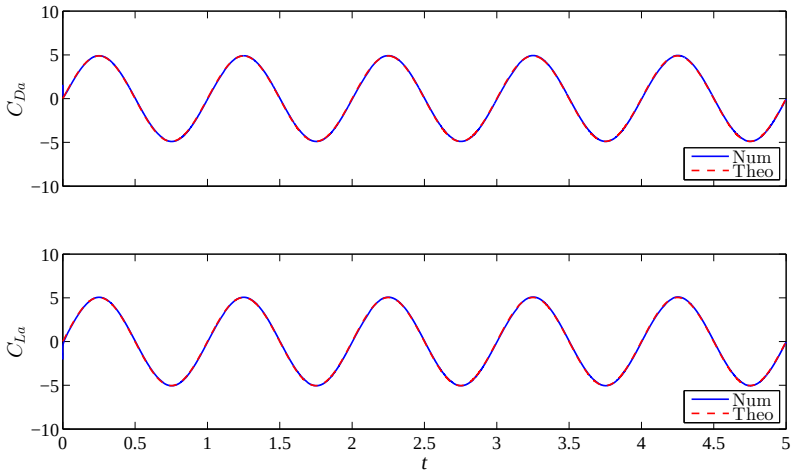

FIG. 25: Comparison of C_{Da} and C_{La} obtained numerically with (A12)-(A13) for an oscillating ellipse with $\epsilon = 1/8$ and $\alpha = 45^o$ for $St_a = 0.16$, $St_c = 1$ and $Re = 500$.

which for a horizontal ellipse ($\alpha = 0$) yields

$$C_{Da} = 0\,, \quad C_{La} = -\frac{\pi}{2}\frac{dV_y}{dt}\,. \tag{A10}$$

Finally, for the heaving motion (5),

$$V_y = \frac{dH}{dt} = 2\pi St_a \cos(2\pi St_c t)\,, \tag{A11}$$

one obtains

$$C_{Da} = 2\pi^3 St_a St_c (1-\epsilon^2)\sin\alpha\cos\alpha\sin(2\pi St_c t)\,, \tag{A12}$$

$$C_{La} = 2\pi^3 St_a St_c (\cos^2\alpha + \epsilon^2\sin^2\alpha)\sin(2\pi St_c t)\,, \tag{A13}$$

and expression (22) when $\alpha = 0$. We checked in several and quite different cases that the numerical results for C_{Da} and C_{La} coincide exactly with these analytical expressions (e.g., Fig. 25). Note that these analytical results for C_{Da} and C_{La} are independent of the Reynolds number.

APPENDIX B: VALIDATION OF THE NUMERICAL CODE

To validate further the numerical code we compare with several published results, and make a mesh convergence analysis for an extreme case among those considered in this work.

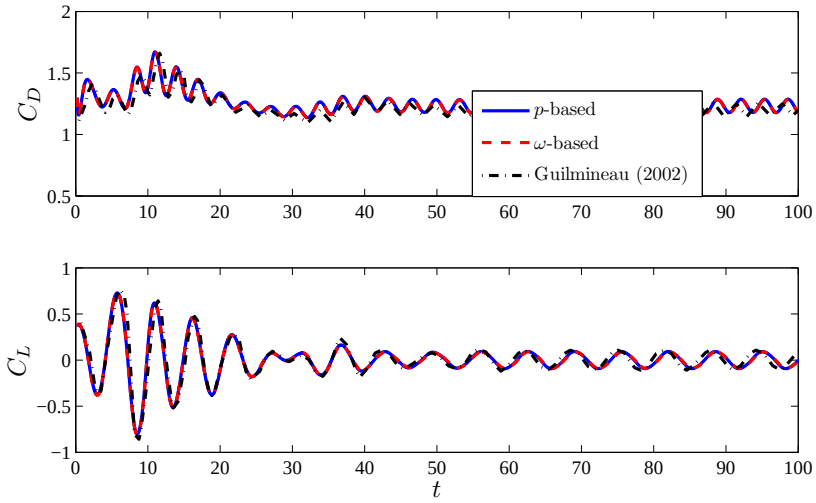

FIG. 26: Comparison of $C_D(t)$ and $C_L(t)$ for an oscillating cylinder ($\epsilon = 1$, $Re = 185$, $St_a = 0.308$, $St_c = 0.154$) with the results by Guilmineau and Queutey[64] [their Fig. 10(a)]. Mesh= 120×100, $\Delta t = 0.002$, $R_o = 25$.

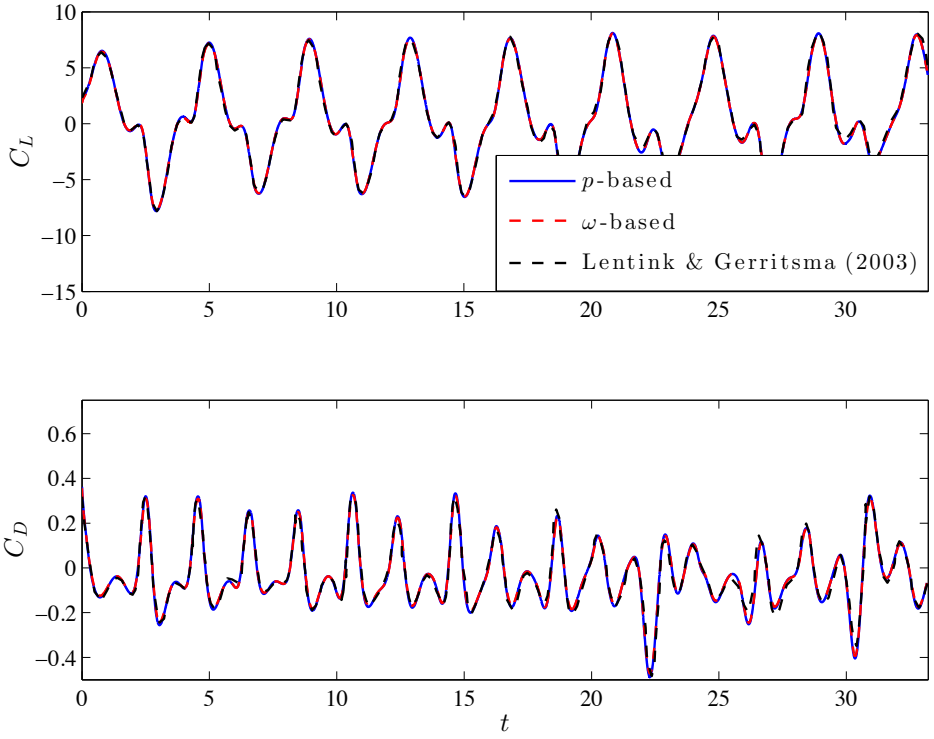

FIG. 27: Comparison of $C_D(t)$ and $C_L(t)$ for an oscillating ellipse ($\epsilon = 0.02$, $Re = 83.2$, $St_a = 0.375$, $St_c = 25$) with the results by Lentink and Gerritsma[34] (their Fig. 25). Mesh= 249×249, $R_o = 25$, $CFL_{max} \leq 0.5$.

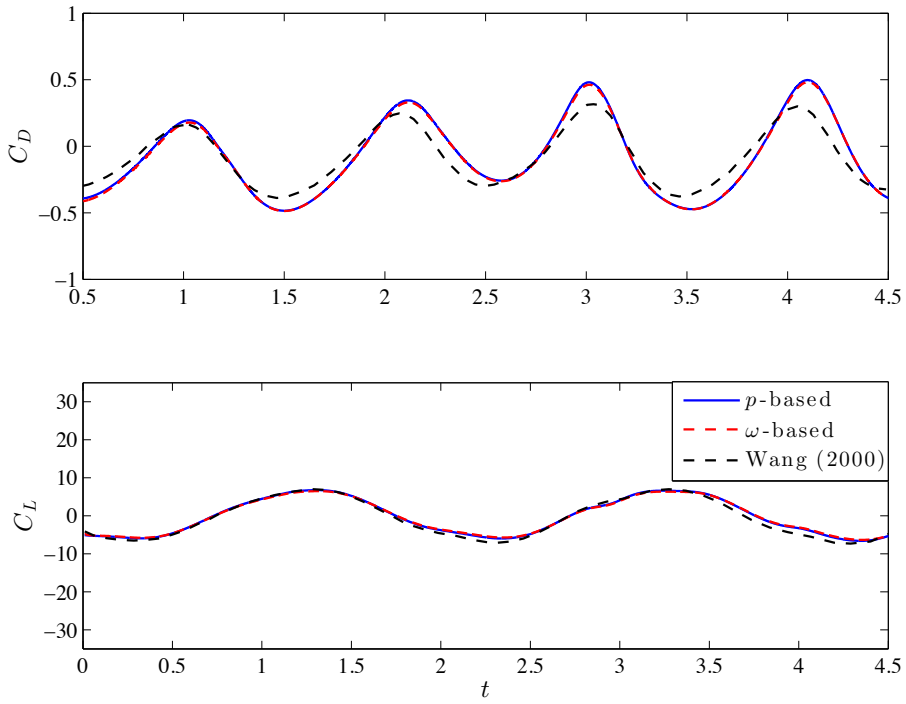

FIG. 28: Comparison of $C_D(t)$ and $C_L(t)$ for an oscillating ellipse ($\epsilon = 1/8$, $Re = 1000$, $St_a = 0.16$, $St_c = 0.5$) with the results by Wang[40] (Fig. 3 of this author). Mesh= 256×256, $R_o = 5$, $CFL_{max} \leq 0.5$.

Figures 26-28 show the temporal evolutions of C_D and C_L for three cases: an oscillating cylinder ($\epsilon = 1$) at $Re = 185$, an oscillating horizontal ($\alpha = 0$) ellipse with $\epsilon = 0.02$ at $Re = 83.2$, and an oscillating horizontal ellipse with $\epsilon = 1/8$ at $Re = 1000$. They are compared with the numerical results by Guilmineau and Queutey,[64] Lentink and Gerritsma,[34] and Wang,[40] respectively. All these researchers validate their numerical codes against some experimental results, and in the three cases we use the same meshes and time steps (when the information is available) as they used in their computations (see figure captions). In spite of the very different numerical methods used (for instance, these authors used non-inertial references frames moving with the oscillating cylinder or ellipse), the agreement is quite good in all cases. In particular, in the case of Fig. 27 the results are practically identical, including the bifurcation in the evolution of C_D at $t \simeq 22.4$.

In these plots we have included the computations of $C_D(t)$ and $C_L(t)$ using both, the pressure-based formulation (8)-(9), and the vorticity-based formulation (12)-(13). It is observed that the results are indistinguishable in all cases, thus validating further the numerical

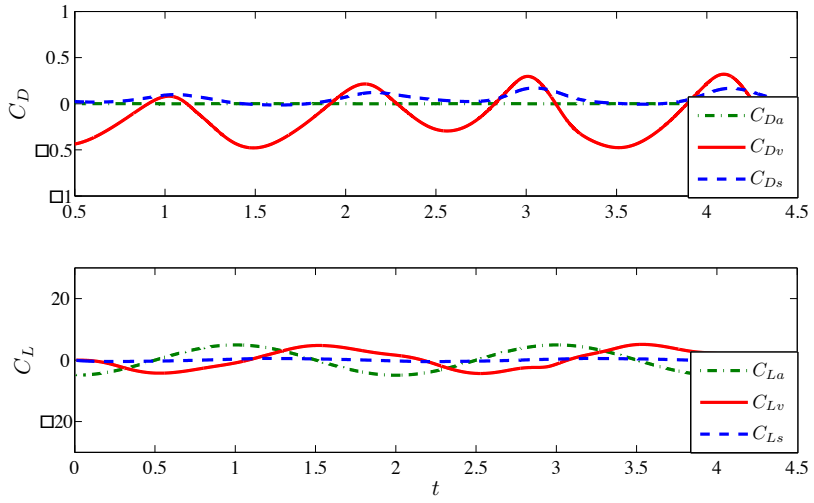

FIG. 29: Different components of $C_D(t)$ and $C_L(t)$ in the vorticity-based formulation (12)-(13) for the same case plotted in Fig. 28.

Mesh	n_θ	n_r	Mesh nodes	$C_{L,max}$	$GCI_{i+1,i}(\%)$	Rel. CPU time
#1	512	512	262144	7.379586	0.670338417	18.9
#2	362	362	131044	7.396075	1.028742892	9.2
#3	256	256	6536	7.421438	1.575745917	3.3
#4	181	181	32761	7.460419	-	1

TABLE I: $C_{L,max}$ for a heaving ellipse with $\epsilon = 1/8$ for $Re = 1000$, $St_a = 0.16$ and $St_c = 0.637$, computed with four meshes of decreasing grid refinement (grid refinement ratio $\varphi = \sqrt{2}$). $R_o = 30$ in all cases. Also shown is the grid convergence index (GCI),[65] and the computation time relative to that using the coarsest grid #4.

implementation of the different integrals used for the computations of these forces in both formulations. As an example, Fig. 29 shows the different components of C_D and C_L in the vorticity force decomposition (12)-(13) for the case computed in Fig. 28.

Finally, to ascertain the effects of the grid refinement on the solution, we consider a heaving ellipse with $\epsilon = 1/8$ at $Re = 1000$ (which is twice the value used in the reported results of Section IV), $St_a = 0.16$ and $St_c = 0.637$ (corresponding to a periodic flow with the heaving frequency). Table I shows the peak value of C_L, once a permanent state is reached,

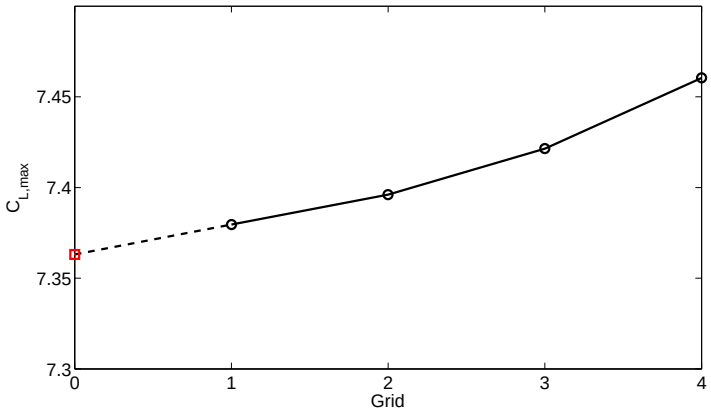

FIG. 30: $C_{L,max}$ computed with the different meshes described in Table I compared with that obtained by the Richardson extrapolation (square), which can be considered as an acceptable approach to the limit value calculated on a mesh with theoretically zero grid spacing.

computed with four meshes of decreasing refinement, with a grid refinement ratio for each coordinate $\varphi = \sqrt{2}$, a computational domain size $R_o = 30$, and a maximum Courant number less or equal than 0.5. Table I includes the grid convergence index (GCI),[65] which is a more conservative measure of the relative error between the solution obtained on a given grid and the asymptotic value than the estimated fractional error derived from the Richardson extrapolation. Nonetheless, Fig. 30 shows the Richardson extrapolation together with the computed values for decreasing grid refinement. From this grid convergence analysis we select the mesh #3 (256×256 grid points) for all the computations reported in the main text, since the GCI is relatively low and the CPU time is about 6 times smaller than with the finest mesh #1.

Acknowledgments

This research has been supported by the *Ministerio de Economía y Competitividad* of Spain Grant No. DPI2013-40479-P, and by the *Junta de Andalucía* Grant No. P10-TEP-5702. The computations have been made in the Picasso Supercomputer at the University of Málaga, a node of the Spanish Supercomputing Network.

---

[1] W. Shyy, H. Aono, C. K. Kang, and H. Liu. *An Introduction to Flapping Wing Aerodynamics*. Cambridge University Press, Cambridge, 2013.

[2] T. Maxworthy. The fluid dynamics of insect flight. *Ann. Rev. Fluid Mech.*, 13:329–350, 1981.

[3] R. Dudley. *The biomechanics of insect flight*. Princeton University Press, Princeton, 2000.

[4] S. P. Sane. The aerodynamics of insect flight. *J. Exp. Biol.*, 206:4191–4208, 2003.

[5] Z. J. Wang. Disecting insect flight. *Ann. Rev. Fluid Mech.*, 37:183–210, 2005.

[6] C. P. Ellington. The novel aerodynamics of insect flight: application to micro-air vehicles. *J. Exp. Biol.*, 202:3439–3448, 1999.

[7] T. J. Mueller. *Fixed and flapping wing aerodynamics for micro air vehicles applications*. AIAA, Reston, 2001.

[8] D. J. Pines and F. Bohorquez. Challenges facing future micro-air-vehicle development. *J. Aircraft*, 43:290–305, 2006.

[9] S. A. Ansari, N. Phillips, G. Stabler, P. C. Wilkins, R. Zbikowski, and K. Knowles. Experimental investigation of some aspects of insect-like flapping flight aerodynamics for application to micro air vehicles. *Exp. Fluids*, 46:777–798, 2009.

[10] K. D. Jones and M. F. Platzer. Design and development considerations for biologically inspired flapping-wing micro air vehicles. *Exp. Fluids*, 46:799–810, 2009.

[11] T. Von Kármán and J. M. Burgers. General aerodynamic theory - Perfect fluids. In W. F. Durand, editor, *Aerodynamic theory*. Springer, Berlin, 1935.

[12] J. B. Bratt. Flow patterns in the wake of an oscillating aerofoil. Technical Report R & M 2773, Aeronautical Research Council, 1950.

[13] T. Y. Wu. Swimming of a waving plate. *J. Fluid Mech.*, 10:321–344, 1961.

[14] M. J. Lighthill. Hydromechanics of aquatic animal propulsion. *Ann. Rev. Fluid Mech.*, 1: 413–449, 1969.

[15] M. J. Lighthill. Aquatic animal propulsion of high hydromechanical efficiency. *J. Fluid Mech.*, 44:265–301, 1970.

[16] M. J. Lighthill. *Mathematical biofluiddynamics*. SIAM, Philadelphia, 1975.

[17] T. Maxworthy. Experiments on the Weis-Foch mechanism of lift generation by insects in hovering flight. Part 1. Dynamics of the 'fling'. *J. Fluid Mech.*, 93:47–63, 1979.

[18] M. H. Dickinson and K. G. Götz. Unsteady aerodynamics performance of model wings at low Reynolds numbers. *J. Exp. Biol.*, 174:45–64, 1993.

[19] C. P. Ellington, C. van den Berg, A. P. Willmott, and A. L. R. Thomas. Leading-edge vortices in insect flight. *Nature*, 384:626–630, 1996.

[20] H. Liu, C. P. Ellington, K. Kawachi, C. van den Berg, and A. P. Willmott. A computational fluid dynamic study of hawkmoth hovering. *J. Exp. Biol.*, 201:561–477, 1998.

[21] S. P. Sane and M. H. Dickinson. The control of flight force by a flapping wing: Lift and drag production. *J. Exp. Biol.*, 204:2607–2626, 2001.

[22] F. O. Minotti. Unsteady two-dimensional theory of a flapping wing. *Phys. Rev. E*, 66:051907, 2002.

[23] T. Maxworthy. The formation and maintenance of a leading-edge vortex during the forward motion of an animal wing. *J. Fluid Mech.*, 587:471–475, 2007.

[24] W. Shyy and H. Liu. Flapping wings and aerodynamic lift: The role of the leading-edge vortex. *AIAA J.*, 45:2817–2819, 2007.

[25] C. W. Pitt and H. Babinsky. Lift and the leading-edge vortex. *J. Fluid Mech.*, 720:280–313, 2013.

[26] K. Streitlien, G. S. Triantafyllou, and M. S. Triantafyllou. Efficient foil propulsion through vortex control. *AIAA J.*, 34:2315–2319, 1996.

[27] J. M. Anderson, K. Streitlien, K. S. Barret, and M. S Triantafyllou. Oscillating foils of high propulsive efficiency. *J. Fluid Mech.*, 360:41–72, 1998.

[28] M. S. Triantafyllou, G. S. Triantafyllou, and D. K. P. Yue. Hydrodynamics of fishlike swimming. *Ann. Rev. Fluid Mech.*, 32:33–53, 2000.

[29] M. S. Triantafyllou, G. S. Triantafyllou, and Grosenbaugh. Optimal thrust development in oscillating foils with application to fish propulsion. *J. Fluid Structures*, 7:205–224, 1993.

[30] K. D. Jones, C. M. Dohring, and M. F. Platzer. Wake structures behind plunging airfoils: A comparison of numerical and experimental results. *AIAA Paper 1996-0078*, 1996.

[31] J. C. S. Lai and M. F. Platzer. Jet characteristics of a plunging airfoil. *AIAA J.*, 37:1529–1537, 1999.

[32] M. M. Koochesfahani. Vortical patterns in the wake of an oscillating airfoil. *AIAA J.*, 27: 1200–1205, 1989.

[33] M. S. Triantafyllou, G. S. Triantafyllou, and R. Gopalkrishnan. Wake mechanics for thrust generation in oscillating foils. *Phys. Fluids A*, 3:2835–2837, 1991.

[34] D. Lentink and M. Gerritsma. Influence of airfoil shape on performance in insect flight. *AIAA Paper 2003-3447*, 2003.

[35] G. K. Taylor, R. L. Nudds, and A. L. R. Thomas. Flying and swimming animals cruise at a Strouhal number tuned for high power efficiency. *Nature*, 425:707–711, 2003.

[36] T. Theodorsen. General theory of aerodynamic instability and the mechanism of flutter. Technical Report TR 496, NACA, 1935.

[37] I. E. Garrick. Propulsion of a flapping and oscillating airfoil. Technical Report TR 567, NACA, 1936.

[38] G. C. Lewin and H. Haj-Hariri. Modelling thrust generation of a two-dimensional heaving airfoil in a viscous flow. *J. Fluid Mech.*, 492:339–362, 2003.

[39] J. O. Dabiri. Optimal vortex formation as a unifying principle in biological propulsion. *Ann. Rev. Fluid Mech.*, 41:17–33, 2009.

[40] Z. J. Wang. Vortex shedding and frequency selection in flapping fight. *J. Fluid Mech.*, 410: 323–341, 2000.

[41] A. Azuma. *Biokinetics of flying and swimming.* AIAA, Washington, 2006.

[42] P. Blondeaux, L. Guglielmini, and M. S. Triantafyllou. Chaotic flow generated by an oscillating foil. *AIAA J.*, 43:918–921, 2005.

[43] K. B. Lua, T. T. Lim, K. S. Yeo, and G. Y. Oo. Wake-structure formation of a heaving two-dimensional elliptic airfoil. *AIAA J.*, 45:1571–1583, 2007.

[44] Z. C. Zheng and Z. Wei. Study of mechanisms and factors that influence the formation of vortical wake of a heaving airfoil. *Phys. Fluids*, 24:103601, 2012.

[45] Z. Wei and Z. C. Zheng. Mechanisms of wake deflection angle change behind heaving airfoil. *J. Fluids Structures*, 48:1–13, 2014.

[46] C.-C. Chang. Potential flow and forces for the incompressible viscous flow. *Proc. R. Soc. A-Math. Phys. Engng Sci.*, 437:517–525, 1992.

[47] J.-J. Lee, C.-T. Hsieh, C. C. Chang, and C.-C. Chu. Vorticity forces on an impulsively started finite plate. *J. Fluid Mech.*, 694:494–492, 2012.

[48] A. Martín-Alcántara, E. Sanmiguel-Rojas, and R. Fernandez-Feria. On the development of lift and drag in a rotating and translating cylinder. *J. Fluids Structures*, 54:868–885, 2015.

[49] L. M. Milne-Thomson. *Theoretical hydrodynamics*. Dover, New York, 1996.

[50] F. M. Bos, B. W. van Oudheusden, and H. Bijl. Radial basis function based mesh deformation applied to simulation of flow around flapping wings. *Computers and Fluids*, 79:167–177, 2013.

[51] R. I. Issa. Solution of the implicitly discretized fluid flow equations by operator-splitting. *J. Comput. Phys.*, 62:40–65, 1985.

[52] P.G. Saffman. *Vortex dynamics*. Cambridge University Press, 1992.

[53] C.-T. Hsieh, C.-C. Kung, C. C. Chang, and C.-C. Chu. Unsteady aerodynamics of a dragonfly using a simple wing-wing model from the perspective of force decomposition. *J. Fluid Mech.*, 663:233–252, 2010.

[54] J. Young and J. C. S. Lai. Mechanisms influencing the efficiency of oscillating airfoil propulsion. *AIAA J.*, 45:1695–1702, 2007.

[55] M. A. Asraf, J. Young, and J. C. S. Lai. Oscillation frequency and amplitude effects on plunging airfoil propulsion and flow periodicity. *AIAA J.*, 50:2308–2324, 2012.

[56] G. J. Li and X. Y. Lu. Force and power of flapping plates in a fluid. *J. Fluid Mech.*, 712: 598–613, 2012.

[57] R. N. Hua, L. Zhu, and X. Y. Lu. Locomotion of a flapping flexible plate. *Phys. Fluids*, 25: 121901, 2013.

[58] F. M. Bos, B. W. van Oudheusden, and H. Bijl. Wing performance and 3-D vortical structure formation in flapping flight. *J. Fluids Structures*, 42:130–151, 2013.

[59] J. Song, H. Luo, and T. L. Hedrick. Three-dimensional flow and lift characteristics of a hovering ruby-throated hummingbird. *J. R. Soc. Interface*, 11:20140541, 2014.

[60] R. B. R. Vandenheede, L. P. Bernal, C. L. Morrison, A. Gogulapati, P. P. Friedmann, C. K. Kang, and W. Shyy. Experimental and computational study on flapping wings with bio-inspired hover kinematics. *AIAA J.*, 52:1047–1058, 2014.

[61] J. W. Jaworski and R. E. Gordnier. Thrust augmentation of flapping airfoils in low Reynolds

number flow using a flexible membrane. *J. Fluids Structures*, 52:199–209, 2015.

[62] P. M. Morse and H. Feshbach. *Methods of theoretical physics*. McGraw-Hill, New York, 1953.

[63] C.-S. Yih. *Fluid Mechanics*. West River Press, Ann Arbor, 1977.

[64] E. Guilmineau and P. Queutey. A numerical simulation of vortex shedding from an oscillating circular cylinder. *J. Fluids Structures*, 16:773–794, 2002.

[65] P. J. Roache. Perspective: a method for uniform reporting of grid refinement studies. *ASME: J. Fluids Eng.*, 116:405413, 1994.